Original Article

An analytical approach on nonlinear mechanical and thermal post-buckling of nanocomposite double-curved shallow shells reinforced by carbon nanotubes

Nguyen Dinh Duc[1,2,3] ⑩, Pham Dinh Nguyen[1], Nguyen Huy Cuong[1], Nguyen Van Sy[1] and Nguyen Dinh Khoa[1]

Abstract

This work presents the nonlinear mechanical and thermal post-buckling of nanocomposite double-curved shallow shells reinforced by single-walled carbon nanotubes resting on elastic foundations based on the higher order shear deformation theory with geometrical nonlinearity in von Karman–Donnell sense. The composite shells are made of various amorphous polymer matrices: poly(methyl methacrylate) (PMMA) and poly{(m-phenylenevinylene)-co-[(2,5-dioctoxy-p-phenylene) vinylene]} (PmPV). The governing equations are solved by the Galerkin method and Airy's stress function to achieve mechanical and thermal post-buckling behaviors of nanocomposite double-curved shallow shells. Various types of distributions of carbon nanotubes, both uniform distributions, and functionally graded distributions are examined. The material properties of nanocomposite double-curved shallow shells are assumed to be temperature dependent. Detailed parametric studies are carried out on the effect of various types of distribution and volume fractions of carbon nanotubes, temperature increments, elastic foundations, edge to radius and edge to thickness ratios on the nonlinear mechanical and thermal post-buckling of nanocomposite double-curved shallow shells reinforced by CNTs.

Keywords

Thermal post-buckling, nanocomposite, double-curved shallow shells, polymer matrices, carbon nanotubes

Date received: 11 May 2018; accepted: 3 September 2018

Introduction

In the past several years, carbon nanotubes (CNTs) have drawn the attention of researchers with regard to science and engineering all over the world. CNTs were first detected by Japanese scientist Sumio Iijima in 1991. CNTs are allotropes of carbon, which have extraordinary properties. Many works have indicated that CNTs have unique mechanical, thermal, electrical properties.[1–7] For example, with 100 times the tensile strength of steel, thermal conductivity is better than all but the purest diamond, and electrical conductivity similar to copper. Since the discovery of CNTs, many experimental and theoretical studies of CNT-reinforced composite structures have significantly increased.

Shen et al.[8–18] investigated the nonlinear buckling and postbuckling, bending static and dynamic response of composite plate and shell structures, which were applied the concept of functionally graded materials for distribution of CNTs in the matrix. Enrique et al.[19] studied the influence of the geometrical variables on the buckling analysis of functionally graded carbon nanotube (FG-CNT) reinforced composite curved subjected to axial compression and shear loads. Duc et al.[20] investigated the nonlinear dynamic response and vibration of imperfect FG-CNT-reinforced composite double-curved shallow shells resting on elastic foundations subjected to blast load based on higher order shear deformation theory (HSDT), Galerkin method, fourth-order

[1]Advanced Materials and Structures Laboratory, VNU University of Engineering and Technology (UET), Hanoi, Vietnam
[2]Infrastructure Engineering Program – VNU-Hanoi, Vietnam-Japan University (VJU), Hanoi, Vietnam
[3]National Research Laboratory, Department of Civil and Environmental Engineering, Sejong University, Seoul, Korea

Corresponding author:
Nguyen Dinh Duc, Advanced Materials and Structures Laboratory, VNU University of Engineering and Technology (UET), Hanoi, Vietnam.
Email: ducnd@vnu.edu.vn

Runge–Kutta method, and Airy's stress function. Mirzaei and Kiani[21] presented free vibration of FG-CNT-reinforced composite cylindrical panels using the first-order shear deformation shell theory (FSDT) and Donnell-type kinematic assumptions. Free vibration characteristics of CNT-reinforced composite spherical panels and dynamics of FG-CNT-reinforced composite cylindrical panel are presented by Kiani[22,23] using Hamilton's principle and the conventional Ritz formulation. Kiani et al.[24] studied the free vibration of FG-CNT-reinforced composite skew cylindrical shells using the Chebyshev–Ritz formulation. The analysis of flexural strength and free vibration of nanocomposite cylindrical panels reinforced by CNTs was investigated by Liew et al.[25] with various types of distributions of CNTs reinforcements and the governing equations are developed based on FSDT. Zhang et al. devoted the large deflection geometrically nonlinear analysis of FG-CNT-reinforced composite cylindrical panels under uniform point transverse mechanical loading using the kp-Ritz method with kernel particle function, which is employed to construct the shape functions for the two-dimensional displacement approximations[26] and the modeling of dynamic responses of CNT-reinforced composite cylindrical shells under impact loads based on Reddy's HSDT.[27]

Zghal et al.[28] investigated the free vibration analysis of FG-CNT-reinforced composite shell structures, where the equations of motion are developed based on discrete double directors shell finite element formulation, which introduces the transverse shear deformations via a higher order distribution of the displacement field. Pouresmaeeli et al.[29] examined the uncertain natural frequencies of moderately thick doubly-curved functionally graded composite panels reinforced by CNTs. Duc et al.[30,31] presented the dynamic response and static stability of FG-CNT-reinforced composite truncated conical shells resting on elastic foundations using the Galerkin method. Asadi[32] presented the numerical simulation of the fluid–solid interaction for CNT-reinforced functionally graded cylindrical shells in thermal environments, where the formulations are derived according to FSDT and Donnell shell theory in conjunction with von Karman geometrical nonlinearity. Trang and Tung[33] presented the thermo-mechanical nonlinear analysis of axially compressed CNT-reinforced composite cylindrical panels resting on elastic foundations with tangentially restrained edges. Ansari et al.[34] investigated the nonlinear post-buckling analysis of piezoelectric FG-CNT-reinforced composite cylindrical shells subjected to combine electro-thermal, axial compression, and lateral loads by applying the Ritz energy approach based on the classical shell theory and the von Karman nonlinear strain–displacement relations of large deformation. Alibeigloo and Pasha Zanoosi[35] investigated the static analysis of FG-CNT-reinforced composite cylindrical shell imbedded in piezoelectric sensor and actuator layers under thermo-electro-mechanical load based on theory of elasticity. Ninh and Bich[36] investigated the electro-thermo-mechanical vibration of FG-CNT-reinforced composite cylindrical shells surrounded by an elastic medium based on geometrical nonlinearity in von Karman–Donnell's sense and the classical shell theory. Lin et al.[37] studied the aeroelastic characteristics and nonlinear response of FG-CNT-reinforced composite panel considering the transient heat conduction.

Moreover, there are a few novel ideas for double-curved shell structures with special approaches. The unified Jacobi–Ritz method is presented and implemented to study the free vibration analysis of coupled composite laminated axis-symmetric doubly-curved revolution shell structures with general boundary conditions in the framework of the FSDT by Cheo et al.[38] Guo et al.[39] investigated the dynamic analysis of composite laminated doubly-curved shells with various boundary conditions by a domain decomposition method with multi-segment partitioning technique is used to establish the formulation based on the FSDT. In Duc et al.,[40,41] a new approach to investigate the nonlinear dynamic response of sandwich auxetic double-curved shallow shells subjected to blast and damping loads based on FSDT and HSDT was considered. Biglari and Jafari[42] addressed the static and free vibration analyses of doubly-curved composite sandwich panels with soft core based on a new three-layered mixed theory. Monterrubio[43] presented the free vibration of shallow shells using the Rayleigh–Ritz method and penalty parameters. Brischetto and Tomabene[44] studied the advanced GDQ models and 3D stress recovery in multilayered plates, spherical, and double-curved panels subjected to transverse shear loads. In Talebitooti and Zarastvand,[45] a diffuse acoustic field was used to analyze the wave propagation on infinite doubly-curved laminated composite shell sandwiching a porous material, which is extensively used in aerospace structures. Mohammad[46] studied the analysis nonlocal electro-elastic bending solution of a doubly-curved piezoelectric nanoshell resting on Winkler–Pasternak foundation based on nonlocal elasticity theory and the first-order shear deformation. Dushyanth et al.[47] presented the dynamic stability of double-curvature composite shells under external blast using Novozhilov nonlinear shell theory and Lagrange's equations of motion. Chen et al.[48] interpreted the free vibration of the functionally graded material (FGM) sandwich doubly-curved shallow shells under simply supported conditions. Using Galerkin method, Duc and Quan[49] analyzed the nonlinear thermal stability of eccentrically stiffened FGM double-curved shallow shells and nonlinear vibration and dynamic response of imperfect FGM double-curved shallow shells with temperature-dependent properties resting on elastic foundations.[50] Pang

et al.[51] presented the free vibration of doubly-curved shells of revolution with arbitrary boundary conditions using a semi-analytical method. Zare et al.[52] devoted the micro- and nano-mechanical behavior of ortho-tropic doubly-curved shells by considering the new modified couple stress theory. Kateryna and Nataliia[53] investigated the stress-deformable state of isotropic double-curved shell with internal cracks and a circular hole.

From the above overview, it is clear that the problems of double-curved shell structures in mechanical structures caught much attention of scientists and researchers. This work proposes the post-buckling behaviors of nanocomposite double-curved shallow shells reinforced by CNTs using analytical methods. The results obtained from post-buckling analysis of FG-CNT-reinforced composite structures will support scientific foundations for structural designers, manufacturers, and for building projects using FG-CNT-reinforced composite structures. The object of this work is to present an analytical approach to obtain the mechanical and thermal post-buckling of FG-CNT-reinforced composite double-curved shallow shells embedded in two different polymer matrices based on the HSDT.

The material properties of CNTs and matrices

The effective material properties of the nanocomposite double-curved shallow shells according to the extended rule of mixture are shown as[8]

$$
\begin{aligned}
E_{11} &= \eta_1 V_{CNT} E_{11}^{CNT} + V_m E_m, \\
\frac{\eta_2}{E_{22}} &= \frac{V_{CNT}}{E_{22}^{CNT}} + \frac{V_m}{E_m}, \\
\frac{\eta_3}{G_{12}} &= \frac{V_{CNT}}{G_{12}^{CNT}} + \frac{V_m}{G_m}
\end{aligned}
\tag{1}
$$

where E_{11}^{CNT}, E_{11}^{CNT}, G_{12}^{CNT} are Young's and shear modulus of CNTs, respectively. E_m, G_m are the mechanical properties of the matrix. V_{CNT} and V_m are the volume fractions of CNTs and the matrix, respectively. $\eta_i (i = \overline{1, 3})$ are the CNTs efficiency parameters.

The effective Poisson's ratio is shown as[8]

$$
v_{12} = V_{CNT}^* v_{12}^{CNT} + V_m v_m
\tag{2}
$$

where Poisson's ratio of the CNTs and the matrix are v_{12}^{CNT}, v_m, respectively.

The thermal expansion coefficients are shown by[13]

$$
\begin{aligned}
\alpha_{11} &= \frac{V_{CNT} E_{11}^{CNT} \alpha_{11}^{CNT} + V_m E_m \alpha_m}{V_{CNT} E_{11}^{CNT} + V_m E_m}, \\
\alpha_{22} &= \left(1 + v_{12}^{CNT}\right) V_{CNT} \alpha_{22}^{CNT} + (1 + v_m) V_m \alpha_m - v_{12} \alpha_{11}
\end{aligned}
\tag{3}
$$

with thermal expansion coefficients of the CNTs being α_{11}^{CNT}, α_{22}^{CNT} and the matrix is α_m.

The material properties of (10,10) SWCNTs, which are dependent on temperature with $v_{12}^{CNT} = 0.175$, are as shown in Table 1.

The FG-CNT-reinforced composite material is made of various polymer matrices reinforced by (10,10) SWCNTs, which are assumed to be aligned and straight with a uniform layout. Uniform distribution (UD) and two types of functionally graded distribution of CNTs (FG-X and FG-O) are considered (Figure 1).

The volume fractions of the CNTs and the matrix are assumed to change according to the linear
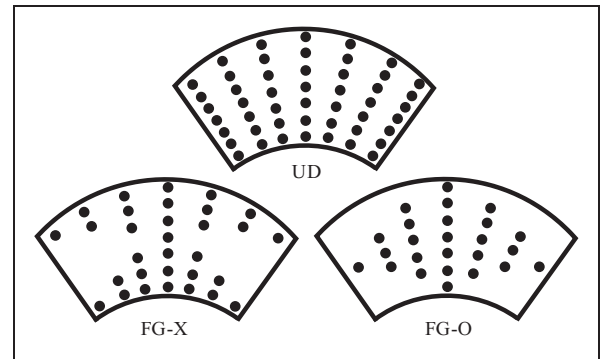

Figure 1. Configurations of CNT-reinforced composite shells.

Table 1. Temperature-dependent material properties for (10, 10) SWCNTs.[15]

T (K)	E_{11}^{CNT} (TPa)	E_{22}^{CNT} (TPa)	G_{12}^{CNT} (TPa)	α_{11}^{CNT} ($\times 10^{-6}$/K)	α_{22}^{CNT} ($\times 10^{-6}$/K)
300	5.6466	7.0800	1.9445	3.4584	5.1682
400	5.5679	6.9814	1.9703	4.1496	5.0905
500	5.5308	6.9348	1.9643	4.5361	5.0189
700	5.4744	6.8641	1.9644	4.6677	4.8943
1000	5.2814	6.6220	1.9451	4.2800	4.7532

$T = T_0 + \Delta T$, ΔT is the temperature increment in the environment containing the material and $T_0 = 300$ K (room temperature).

Table 2. The material properties of the PMMA and PmPV matrices.

Matrix	E_m(GPa)	v_m	$\alpha_m(\times 10^{-6}/K)$
PMMA	$(3.52 - 0.0034\Delta T)$	0.34	$45(1 + 0.0005\Delta T)$
PmPV	$(3.51 - 0.0047\Delta T)$	0.34	$45(1 + 0.0005\Delta T)$

Table 3. CNTs efficiency parameters for (10,10) SWCNT-reinforced composites.

	V^*_{CNT}	η_1	η_2	η_3
PMMA/CNT	0.12	0.137	1.022	0.715
composites	0.17	0.142	1.626	1.138
	0.28	0.141	1.585	1.110
PmPV/CNT	0.11	0.149	0.934	0.654
composites	0.14	0.150	0.941	0.659
	0.17	0.149	1.381	0.967

functions of the shell thickness as follows[8]

$$V_{CNT} = \begin{cases} V^*_{CNT} & (UD) \\ 4V^*_{CNT}\frac{|z|}{h} & (FG\text{-}X), \\ 2V^*_{CNT}\left(1 - 2\frac{|z|}{h}\right) & (FG\text{-}O) \end{cases} \quad V_m = 1 - V_{CNT}$$

(4)

in which

$$V^*_{CNT} = \frac{w_{CNT}}{w_{CNT} + (\rho_{CNT}/\rho_m) - (\rho_{CNT}/\rho_m)w_{CNT}}$$

(5)

with w_{CNT} being the mass fraction of CNTs, and ρ_{CNT} and ρ_m are the densities of CNTs and matrix, respectively.
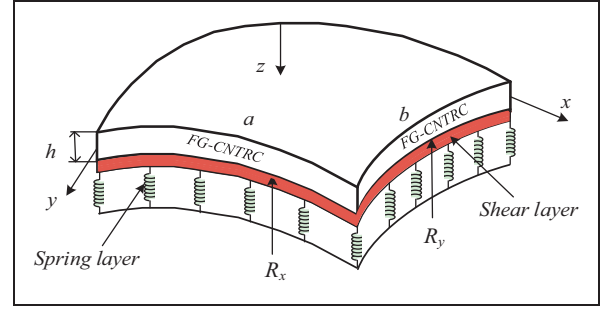
The nanocomposite double-curved shallow shells are embedded in two amorphous polymer matrices: poly(methyl methacrylate) (PMMA) and poly{(m-phenylenevinylene)-co-[(2,5-dioctoxy-p-phenylene) vinylene]} (PmPV). The material properties are shown in Table 2.[8,9]

The $\eta_i\,(i = \overline{1,3})$ used in equation (1) are obtained by molecular dynamics (MD) simulation results of model polymer/CNTs composites, which are presented in Table 3.[8,9]

Theoretical formulations

Consider an FG-CNT-reinforced composite double-curved shallow shell with length of edges a, b, radii of curvature R_x, R_y, and thickness h. A coordinate system (x, y, z) is derived in which (x, y) plane on the middle surface of the shell and z on thickness direction $(-h/2 \leqslant z \leqslant h/2)$ is as shown in Figure 2.

The post-buckling of nanocomposite double-curved shallow shells reinforced by CNTs are derived by Galerkin method based on HSDT. The strain

Figure 2. Geometry and coordinate system of nanocomposite double-curved shallow shells resting on elastic foundations. FG-CNTRC: functionally graded carbon nanotube reinforced composite.

components taking into account von Karman nonlinear terms are given by[54]

$$\begin{pmatrix} \varepsilon_x \\ \varepsilon_y \\ \gamma_{xy} \end{pmatrix} = \begin{pmatrix} \varepsilon^0_x \\ \varepsilon^0_y \\ \gamma^0_{xy} \end{pmatrix} + z\begin{pmatrix} k^1_x \\ k^1_y \\ k^1_{xy} \end{pmatrix} + z^3\begin{pmatrix} k^3_x \\ k^3_y \\ k^3_{xy} \end{pmatrix},$$

$$\begin{pmatrix} \gamma_{xz} \\ \gamma_{yz} \end{pmatrix} = \begin{pmatrix} \gamma^0_{xz} \\ \gamma^0_{yz} \end{pmatrix} + z^2\begin{pmatrix} k^2_{xz} \\ k^2_{yz} \end{pmatrix}$$

(6)

where

$$\begin{pmatrix} \varepsilon^0_x \\ \varepsilon^0_y \\ \gamma^0_{xy} \end{pmatrix} = \begin{pmatrix} u_{,x} - w/R_x + w^2_{,x}/2 \\ v_{,y} - w/R_y + w^2_{,y}/2 \\ u_{,y} + v_{,x} + w_{,x}w_{,y} \end{pmatrix}, \begin{pmatrix} \gamma^0_{xz} \\ \gamma^0_{yz} \end{pmatrix} = \begin{pmatrix} \phi_x + w_{,x} \\ \phi_y + w_{,y} \end{pmatrix}$$

(7)

$$\begin{pmatrix} k^1_x \\ k^1_y \\ k^1_{xy} \end{pmatrix} = \begin{pmatrix} \phi_{x,x} \\ \phi_{y,y} \\ \phi_{x,y} + \phi_{y,x} \end{pmatrix}, \begin{pmatrix} k^2_{xz} \\ k^2_{yz} \end{pmatrix} = -3c_1\begin{pmatrix} \phi_x + w_{,x} \\ \phi_y + w_{,y} \end{pmatrix},$$

$$\begin{pmatrix} k^3_x \\ k^3_y \\ k^3_{xy} \end{pmatrix} = -c_1\begin{pmatrix} \phi_{x,x} + w_{,xx} \\ \phi_{y,y} + w_{,yy} \\ \phi_{x,y} + \phi_{y,x} + 2w_{,xy} \end{pmatrix}$$

(8)

The strain–stress relations are defined as

$$\begin{Bmatrix} \sigma_x \\ \sigma_y \\ \sigma_{yz} \\ \sigma_{xz} \\ \sigma_{xy} \end{Bmatrix} = \begin{vmatrix} Q_{11} & Q_{12} & 0 & 0 & 0 \\ Q_{12} & Q_{22} & 0 & 0 & 0 \\ 0 & 0 & Q_{55} & 0 & 0 \\ 0 & 0 & 0 & Q_{44} & 0 \\ 0 & 0 & 0 & 0 & Q_{66} \end{vmatrix}$$

$$\times \left[\begin{Bmatrix} \varepsilon_x \\ \varepsilon_y \\ \gamma_{yz} \\ \gamma_{xz} \\ \gamma_{xy} \end{Bmatrix} - \Delta T \begin{Bmatrix} \alpha_{11} \\ \alpha_{22} \\ 0 \\ 0 \\ 0 \end{Bmatrix} \right]$$

(9)

where

$$Q_{11} = \frac{E_{11}}{1 - v_{12}v_{21}}, \quad Q_{12} = \frac{v_{21}E_{11}}{1 - v_{12}v_{21}},$$

$$Q_{22} = \frac{E_{22}}{1 - v_{12}v_{21}}, \quad Q_{44} = G_{23}, \quad Q_{55} = G_{13},$$

$$Q_{66} = G_{12}$$

(10)

The nonlinear equilibrium equation of the shells are shown as[49,54]

$$
\begin{Bmatrix} N_x \\ N_y \\ N_{xy} \\ M_x \\ M_y \\ M_{xy} \\ P_x \\ P_y \\ P_{xy} \end{Bmatrix}
=
\begin{bmatrix}
A_{11} & A_{12} & 0 & B_{11} & B_{12} & 0 & F_{11} & F_{12} & 0 \\
A_{12} & A_{22} & 0 & B_{12} & B_{22} & 0 & F_{12} & F_{22} & 0 \\
0 & 0 & A_{66} & 0 & 0 & B_{66} & 0 & 0 & F_{66} \\
B_{11} & B_{12} & 0 & D_{11} & D_{12} & 0 & H_{11} & H_{12} & 0 \\
B_{12} & B_{22} & 0 & D_{12} & D_{22} & 0 & H_{12} & H_{22} & 0 \\
0 & 0 & B_{66} & 0 & 0 & D_{66} & 0 & 0 & H_{66} \\
F_{11} & F_{12} & 0 & H_{11} & H_{12} & 0 & O_{11} & O_{12} & 0 \\
F_{12} & F_{22} & 0 & H_{12} & H_{22} & 0 & O_{12} & O_{22} & 0 \\
0 & 0 & F_{66} & 0 & 0 & H_{66} & 0 & 0 & O_{66}
\end{bmatrix}
\begin{Bmatrix} \varepsilon_x^0 \\ \varepsilon_y^0 \\ \gamma_{xy}^0 \\ k_x^1 \\ k_y^1 \\ k_{xy}^1 \\ k_x^3 \\ k_y^3 \\ k_{xy}^3 \end{Bmatrix}
-
\begin{Bmatrix} N_x^T \\ N_y^T \\ 0 \\ M_x^T \\ M_y^T \\ 0 \\ P_x^T \\ P_y^T \\ 0 \end{Bmatrix},
$$

(13)

$$
\begin{Bmatrix} Q_x \\ Q_y \\ K_x \\ K_y \end{Bmatrix}
=
\begin{bmatrix}
A_{44} & 0 & D_{44} & 0 \\
0 & A_{55} & 0 & D_{55} \\
D_{44} & 0 & H_{44} & 0 \\
0 & D_{55} & 0 & H_{55}
\end{bmatrix}
\begin{Bmatrix} \gamma_{xz}^0 \\ \gamma_{yz}^0 \\ k_{xz}^2 \\ k_{yz}^2 \end{Bmatrix}
$$

$$N_{x,x} + N_{xy,y} = 0 \tag{11a}$$

$$N_{xy,x} + N_{y,y} = 0 \tag{11b}$$

$$Q_{x,x} + Q_{y,y} - 3c_1\left(K_{x,x} + K_{y,y}\right)$$
$$+ c_1\left(P_{x,xx} + 2P_{xy,xy} + P_{y,yy}\right) + \frac{N_x}{R_x} + \frac{N_y}{R_y}$$
$$+ N_x w_{,xx} + 2N_{xy}w_{,xy} + N_y w_{,yy}$$
$$+ q - K_w w + K_p \nabla^2 w = 0 \tag{11c}$$

$$M_{x,x} + M_{xy,xy} - Q_x + 3c_1 K_x - c_1\left(P_{x,x} + P_{xy,y}\right) = 0 \tag{11d}$$

$$M_{xy,x} + M_{y,y} - Q_y + 3c_1 K_y - c_1\left(P_{xy,x} + P_{y,y}\right) = 0 \tag{11e}$$

with K_w (GPa/m) is Winkler foundation modulus, K_p (GPa·m) is the shear layer foundation stiffness of Pasternak model, and q is a uniformly distributed external pressure.

The force and moment components of nanocomposite double-curved shallow shells reinforced by CNTs are shown as

$$(N_i, M_i, P_i) = \int_{-h2}^{h2} \sigma_i(1, z, z^3)dz, \quad \{i = x, y, xy\},$$

$$(Q_i, K_i) = \int_{-h2}^{h2} \sigma_j(1, z^2)dz, \quad \{i = x, y; j = xz, yz\}$$

(12)

Substituting equations (6) and (9) into equations (12) leads to the constitutive relations, which can be written as

where

$$\left(A_{ij}, B_{ij}, D_{ij}, F_{ij}, H_{ij}, L_{ij}, O_{ij}\right)$$
$$= \int_{-\frac{h}{2}}^{\frac{h}{2}} \left(Q_{ij}, zQ_{ij}, z^2Q_{ij}, z^3Q_{ij}, z^4Q_{ij}, z^5Q_{ij}, z^6Q_{ij}\right)dz,$$

$$(N_x^T, M_x^T, P_x^T) = \int_{-\frac{h}{2}}^{\frac{h}{2}} (Q_{11}\alpha_{11} + Q_{12}\alpha_{22})(1, z, z^3)\Delta T dz,$$

$$(N_y^T, M_y^T, P_y^T) = \int_{-\frac{h}{2}}^{\frac{h}{2}} (Q_{12}\alpha_{11} + Q_{22}\alpha_{22})(1, z, z^3)\Delta T dz$$

(14)

From the constitutive relations (13), the reverse relations are obtained as

$$
\begin{Bmatrix} \varepsilon_x^0 \\ \varepsilon_y^0 \\ \gamma_{xy}^0 \end{Bmatrix}
=
\begin{bmatrix}
-I_{12} & I_{11} & 0 \\
I_{22} & -I_{12} & 0 \\
0 & 0 & -I_{31}
\end{bmatrix}
\begin{Bmatrix} f_{,xx} \\ f_{,yy} \\ f_{,xy} \end{Bmatrix}
$$

$$+ \begin{bmatrix} I_{13} & I_{14} & 0 \\ I_{23} & I_{24} & 0 \\ 0 & 0 & I_{32} \end{bmatrix} \begin{Bmatrix} \phi_{x,x} \\ \phi_{y,y} \\ (\phi_{x,y} + \phi_{y,x}) \end{Bmatrix}$$
$$- c_1 \begin{bmatrix} I_{15} & I_{16} & 0 \\ I_{25} & I_{26} & 0 \\ 0 & 0 & I_{33} \end{bmatrix} \begin{Bmatrix} (w_{,xx} + \phi_{x,x}) \\ (w_{,yy} + \phi_{y,y}) \\ (2w_{,xy} + \phi_{x,y} + \phi_{y,x}) \end{Bmatrix}$$
$$+ \begin{bmatrix} I_{11} & -I_{12} & 0 \\ -I_{12} & I_{22} & 0 \\ 0 & 0 & 0 \end{bmatrix} \begin{Bmatrix} N_x^T \\ N_y^T \\ 0 \end{Bmatrix} \qquad (15)$$

in which

$$\Delta = A_{11}A_{22} - A_{12}^2, \quad I_{11} = \frac{A_{22}}{\Delta}, \quad I_{12} = \frac{A_{12}}{\Delta},$$
$$I_{13} = \frac{A_{12}B_{12} - A_{22}B_{11}}{\Delta}, \quad I_{14} = \frac{A_{12}B_{22} - A_{22}B_{12}}{\Delta},$$
$$I_{15} = \frac{A_{12}F_{12} - A_{22}F_{11}}{\Delta}, \quad I_{16} = \frac{A_{12}F_{22} - A_{22}F_{12}}{\Delta},$$
$$I_{22} = \frac{A_{11}}{\Delta}, \quad I_{23} = \frac{A_{12}B_{11} - A_{11}B_{12}}{\Delta},$$
$$I_{24} = \frac{A_{12}B_{12} - A_{11}B_{22}}{\Delta}, \quad I_{25} = \frac{A_{12}F_{11} - A_{11}F_{12}}{\Delta},$$
$$I_{26} = \frac{A_{12}F_{12} - A_{11}F_{22}}{\Delta}, \quad I_{31} = \frac{1}{A_{66}},$$
$$I_{32} = -\frac{B_{66}}{A_{66}}; \quad I_{33} = -\frac{F_{66}}{A_{66}}$$
$$(16)$$

and Airy's stress function $f(x,y)$ is determined as

$$N_x = f_{,yy}, \quad N_y = f_{,xx}, \quad N_{xy} = -f_{,xy} \qquad (17)$$

The geometrical compatibility equation for an imperfect double-curved shallow shell is shown as

$$\varepsilon_{x,yy}^0 + \varepsilon_{y,xx}^0 - \gamma_{xy,xy}^0 = w_{,xy}^2 - w_{,xx}w_{,yy} + 2w_{,xy}w_{,xy}^*$$
$$- w_{,xx}w_{,yy}^* - w_{,yy}w_{,xx}^*$$
$$- \frac{w_{,yy}}{R_x} - \frac{w_{,xx}}{R_y}$$
$$(18)$$

where $w^*(x,y)$ is the imperfection function and denotes initial small imperfection of the shell.

Substituting equation (15) with Airy's stress function into equation (13) results in equations (11c) to (11e) to be written as

$$L_{11}(w) + L_{12}(\phi_x) + L_{13}(\phi_y) + L_{14}(f)$$
$$+ P_1(w,f) + L_{11}(w^*) + P_1'(w^*,f) + q = 0,$$
$$L_{21}(w) + L_{22}(\phi_x) + L_{23}(\phi_y) + P_2(f) + L_{21}(w^*) = 0,$$
$$L_{31}(w) + L_{32}(\phi_x) + L_{33}(\phi_y) + P_3(f) + L_{31}(w^*) = 0$$
$$(19)$$

where

$$L_{11}(w) = U_{11}w_{,xx} + U_{12}w_{,yy} + U_{13}w_{,xxxx}$$
$$+ U_{14}w_{,xxyy} + U_{15}w_{,yyyy} - k_w w + k_p \nabla^2 w,$$
$$L_{12}(\phi_x) = U_{11}\phi_{x,x} + U_{16}\phi_{x,xxx} + U_{17}\phi_{x,xyy},$$
$$L_{13}(\phi_y) = U_{12}\phi_{y,y} + U_{18}\phi_{y,yyy} + U_{19}\phi_{y,xxy},$$
$$L_{14}(f) = U_{110}f_{,xxxx} + U_{111}f_{,xxyy} + U_{112}f_{,yyyy},$$
$$L_{21}(w) = U_{21}w_{,x} + U_{22}w_{,xxx} + U_{23}w_{,xyy},$$
$$L_{22}(\phi_x) = U_{21}\phi_x + U_{24}\phi_{x,xx} + U_{25}\phi_{x,yy},$$
$$L_{23}(\phi_y) = U_{26}\phi_{y,xy},$$
$$L_{31}(w) = U_{31}w_{,y} + U_{32}w_{,xxy} + U_{33}w_{,yyy},$$
$$L_{32}(\phi_x) = U_{34}\phi_{x,xy},$$
$$L_{33}(\phi_y) = U_{31}\phi_y + U_{35}\phi_{y,xx} + U_{36}\phi_{y,yy},$$
$$P_1(w,f) = \frac{f_{,yy}}{R_x} + \frac{f_{,xx}}{R_y} + f_{,yy}w_{,xx} - 2f_{,xy}w_{,xy}$$
$$+ f_{,xx}w_{,yy},$$
$$P_2(f) = U_{27}f_{,xxx} + U_{28}f_{,xyy},$$
$$P_3(f) = U_{37}f_{,xxy} + U_{38}f_{,yyy},$$
$$L_{11}^*(w^*) = U_{11}w_{,xx}^* + U_{12}w_{,yy}^*,$$
$$P_1'(w^*,f) = f_{,yy}w_{,xx}^* - 2f_{,xy}w_{,xy}^* + f_{,xx}w_{,yy}^*,$$
$$L_{21}^*(w^*) = U_{21}w_{,x}^*, \quad L_{31}^*(w^*) = U_{31}w_{,y}^*$$
$$(20)$$

and the coefficients $U_{1i}(i = \overline{1 \div 12})$, $U_{2j}(i = \overline{1 \div 8})$, $U_{3k}(k = \overline{1 \div 8})$ are shown in Appendix 1.

Substitution of equations (15) into equation (18) leads to

$$I_{21}f_{,xxxx} + I_{11}f_{,yyyy} + J_1 f_{,xxyy} + J_2\phi_{x,xxx} + J_3\phi_{x,xyy}$$
$$+ J_4\phi_{y,yyy} + J_5\phi_{y,xxy} - c_1 I_{25}w_{,xxxx} - c_1 I_{16}w_{,yyyy}$$
$$+ J_6 w_{,xxyy} = w_{,xy}^2 - w_{,xx}w_{,yy} + 2w_{,xy}w_{,xy}^*$$
$$- w_{,xx}w_{,yy}^* - w_{,yy}w_{,xx}^* - \frac{w_{,yy}}{R_x} - \frac{w_{,xx}}{R_y}$$
$$(21)$$

in which

$$J_1 = I_{31} - 2I_{12}, \quad J_2 = I_{23} - c_1 I_{25},$$
$$J_3 = I_{13} - c_1 I_{15} - I_{32} + c_1 I_{33}, \quad J_4 = I_{14} - c_1 I_{16},$$
$$J_5 = I_{24} - c_1 I_{26} - I_{32} + c_1 I_{33},$$
$$J_6 = -c_1 I_{15} - c_1 I_{26} + 2c_1 I_{33}$$

Equations (19) and (21) are used to study post-buckling of nanocomposite double-curved shallow shells reinforced by CNTs based on HSDT.

Analytical solution

The double-curved shallow shells are assumed to be simply supported. Two cases of boundary conditions are considered.[50,54]

Case 1: Edges of the shell are immovable

$$w = u = \phi_y = M_x = P_x = 0, \quad N_x = N_{x0} \quad \text{at} \quad x = 0, a,$$
$$w = v = \phi_x = M_y = P_y = 0, \quad N_y = N_{y0} \quad \text{at} \quad y = 0, b$$
(22a)

Case 2: Edges of the shell are freely movable

$$w = N_{xy} = \phi_y = M_x = P_x = 0, \quad N_x = N_{x0} \quad \text{at} \quad x = 0, a,$$
$$w = N_{xy} = M_y = P_y = 0, N_y = N_{y0} \quad \text{at} \quad y = 0, b$$
(22b)

where N_{x0}, N_{y0} are fictitious compressive edge loads at immovable edges and in-plane compressive loads at movable edges.

The approximate solutions of the shells satisfied boundary conditions can be shown as[20]

$$\begin{bmatrix} w(x, y) \\ \phi_x(x, y) \\ \phi_y(x, y) \\ w^*(x, y) \end{bmatrix} = \begin{bmatrix} W \sin \lambda_m x \sin \delta_n y \\ \Phi_x \cos \lambda_m x \sin \delta_n y \\ \Phi_y \sin \lambda_m x \cos \delta_n y \\ \mu h \sin \lambda_m x \cos \delta_n y \end{bmatrix}$$
(23)

where $\lambda_m = m\pi/a$, $\delta_n = n\pi/b$, and m, n are the number of half waves in the x and y directions, respectively. μ is the imperfection parameter of the shells.

Substituting equations (23) into equation (21) leads to

$$f = A_1 \cos 2\lambda_m x + A_2 \cos 2\delta_n y + A_3 \sin \lambda_m x \sin \delta_n y$$
$$+ \frac{1}{2} N_{xo} y^2 + \frac{1}{2} N_{yo} x^2$$
(24)

in which

$$A_1 = \frac{\delta_n^2}{32 I_{22} \lambda_m^2} W(W + 2\mu h),$$

$$A_2 = \frac{\lambda_m^2}{32 I_{11} \delta_n^2} W(W + 2\mu h), \quad A_3 = P_1 W + P_2 \phi_x + P_3 \phi_y,$$

$$P_1 = \frac{\left(c_1 I_{25} \lambda_m^4 - J_6 \lambda_m^2 \delta_n^2 + c_1 I_{16} \delta_n^4 + \frac{\delta_n^2}{R_x} + \frac{\lambda_m^2}{R_y} \right)}{P_D},$$

$$P_2 = \frac{-\left(J_2 \lambda_m^3 + J_3 \lambda_m \delta_n^2 \right)}{P_D},$$

$$P_3 = \frac{-\left(J_4 \delta_n^3 + J_5 \lambda_m^2 \delta_n \right)}{P_D}, P_D = I_{22} \lambda_m^4 + I_{11} \delta_n^4 + J_1 \lambda_m^2 \delta_n^2$$

Introducing equations (23) and (24) into equations (19) and then applying Galerkin method the following equations can be obtained

$$l_{11} W + l_{12} \phi_x + l_{13} \phi_y + l_{14}(W + \mu h)\phi_x + l_{15}(W + \mu h)\phi_y$$
$$+ \left[n_1 - \left(N_{x0} \lambda_m^2 + N_{y0} \delta_n^2 \right) \right](W + \mu h) + n_2 W(W + \mu h)$$
$$+ n_3 W(W + 2\mu h) + n_4 W(W + \mu h)(W + 2\mu h)$$

$$+ n_5 \left(\frac{N_{x0}}{R_x} + \frac{N_{y0}}{R_y} \right) + n_5 q = 0,$$
$$l_{21} W + l_{22} \phi_x + l_{23} \phi_y + n_6(W + \mu h) + n_7 W(W + 2\mu h) = 0,$$
$$l_{31} W + l_{32} \phi_x + l_{33} \phi_y + n_8(W + \mu h) + n_9 W(W + 2\mu h) = 0,$$
(25)

with the details of coefficients $l_{1i}(i = \overline{1 \div 3}), l_{jk}(j = \overline{2 \div 3}, k = \overline{1 \div 3}), n_q(q = \overline{1 \div 9})$ shown in Appendix 2.

Consider a simply supported nanocomposite double-curved shallow shell with all immovable edges (i.e. $u = 0$ at $x = 0$, a and $v = 0$ at $y = 0$, b)

$$\int_0^b \int_0^a \frac{\partial u}{\partial x} \mathrm{d}x \, \mathrm{d}y = 0, \quad \int_0^a \int_0^b \frac{\partial v}{\partial y} \mathrm{d}y \mathrm{d}x = 0 \quad (26)$$

Substituting equations (15) into equations (7) results in the following expressions

$$\left\{ \begin{array}{c} \frac{\partial u}{\partial x} \\ \frac{\partial v}{\partial y} \end{array} \right\} = \begin{bmatrix} -I_{12} & I_{11} \\ I_{22} & -I_{12} \end{bmatrix} \left\{ \begin{array}{c} f_{,xx} \\ f_{,yy} \end{array} \right\} + \begin{bmatrix} I_{13} & I_{14} \\ I_{23} & I_{24} \end{bmatrix}$$

$$\times \left\{ \begin{array}{c} \phi_{x,x} \\ \phi_{y,y} \end{array} \right\} - c_1 \begin{bmatrix} I_{15} & I_{16} \\ I_{25} & L_{26} \end{bmatrix} \left\{ \begin{array}{c} (w_{,xx} + \phi_{x,x}) \\ (w_{,yy} + \phi_{y,y}) \end{array} \right\}$$

$$+ \begin{bmatrix} I_{11} & -I_{12} \\ -I_{12} & I_{21} \end{bmatrix} \left\{ \begin{array}{c} N_x^T \\ N_y^T \end{array} \right\} + \begin{bmatrix} \frac{w}{R_x} - w_{,x} w_{,x}^* - \frac{w_{,x}^2}{2} \\ \frac{w}{R_y} - w_{,y} w_{,y}^* - \frac{w_{,y}^2}{2} \end{bmatrix}$$
(27)

Introduction of equations (27) into equation (26) leads to

$$\begin{bmatrix} N_{x0} \\ N_{y0} \end{bmatrix} = \begin{bmatrix} m_1 & m_4 \\ m_1^* & m_4^* \end{bmatrix} \left\{ \begin{array}{c} W \\ W(W + 2\mu h) \end{array} \right\}$$
$$+ \begin{bmatrix} m_2 & m_3 \\ m_2^* & m_3^* \end{bmatrix} \left\{ \begin{array}{c} \phi_x \\ \phi_y \end{array} \right\} + \begin{bmatrix} m_5 & m_6 \\ m_5^* & m_6^* \end{bmatrix} \left\{ \begin{array}{c} N_x^T \\ N_y^T \end{array} \right\}$$
(28)

with the coefficients $m_i(i = \overline{1 \div 6})$, $m_i^*(i = \overline{1 \div 6})$ shown in Appendix 3.

Using the second and third equations of the system of equations (25) leads to

$$\phi_x = \frac{\left\{ \begin{array}{c} [(n_9 l_{23} - n_7 l_{33})W(W + 2\mu h) + (n_8 l_{23} - n_6 l_{33}) \\ (W + \mu h) + (l_{23} l_{31} - l_{21} l_{33})W] \end{array} \right\}}{(l_{22} l_{33} - l_{23} l_{32})},$$

$$\phi_y = \frac{\left\{ \begin{array}{c} [(n_9 l_{22} - n_7 l_{32})W(W + 2\mu h) + (n_8 l_{22} - n_6 l_{32}) \\ (W + \mu h) + (l_{22} l_{31} - l_{21} l_{32})W] \end{array} \right\}}{(l_{23} l_{32} - l_{22} l_{33})}$$
(29)

Substitution of equations (28) and (29) into the first of the system of equations (25) results in obtaining of the equation to investigate the mechanical

post-buckling of nanocomposite double-curved shallow shells

$$
\begin{aligned}
q = {}& b_1^1 W_n (W_n + \mu)(W_n + 2\mu) + b_1^2 (W_n + \mu)(W_n + \mu) \\
& + b_1^3 W_n (W_n + 2\mu) + b_1^4 W_n (W_n + \mu) \\
& + b_1^5 (W_n + \mu) + b_1^6 W_n + b_1^7 N_x^T + b_1^8 N_y^T
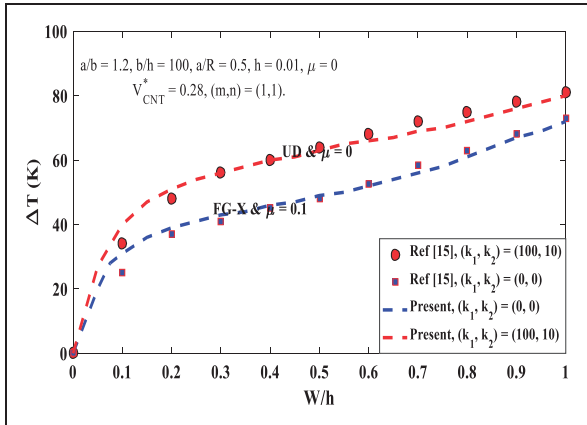\end{aligned}
$$

(30)

Figure 3. Comparison of thermal post-buckling behavior of nanocomposite cylindrical panels.
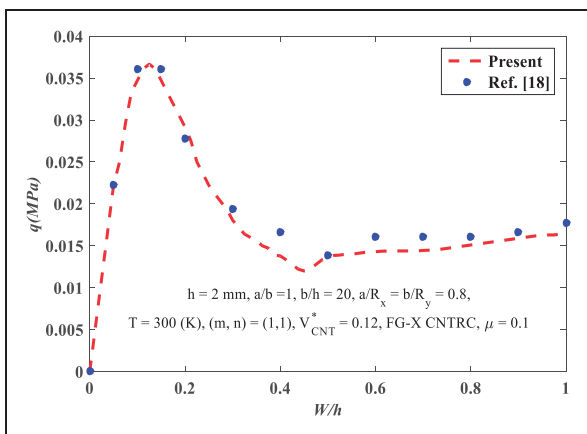

Figure 4. Comparison of mechanical post-buckling behavior of nanocomposite double-curved panels.

Introduction of equations (28) and (29) into the first of the system of equations (25) taking into account the temperature increment ΔT in equation (12), the equation to investigate thermal post-buckling of nanocomposite double-curved shallow shells is obtained

$$
\begin{aligned}
\Delta T = {}& b_2^1 W_n (W_n + \mu)(W_n + 2\mu) + b_2^2 (W_n + \mu)(W_n + \mu) \\
& + b_2^3 W_n (W_n + 2\mu) + b_2^4 W_n (W_n + \mu) \\
& + b_2^5 (W_n + \mu) + b_2^6 W_n + b_2^7
\end{aligned}
$$

(31)

with the coefficients $b_i^k \left(i = \overline{1 \div 2}, k = \overline{1 \div 8} \right)$ are shown in Appendix 4.

Numerical results and discussion

Comparison

To validate the formulation in this work, comparisons are carried out for the post-buckling behavior of nanocomposite cylindrical panels (Figure 3) and double-curved panels (Figure 4) reinforced by CNTs with Shen's results.[15,18] In Figure 3, the geometrical parameters are taken to be $a/b = 1, b/h = 100$, $a/R = 0.5$, the volume fraction of CNTs is taken to be $V_{CNT}^* = 0.28$. Figure 3 shows the thermal post-buckling behavior of perfect nanocomposite cylindrical panels resting on the elastic foundation with UD type and imperfect nanocomposite cylindrical panels with FG-X type. Figure 4 compares the mechanical post-buckling behavior of imperfect FG-X CNT-reinforced composite double-curved panels with the same geometrical and material parameters. It is clear that the analytical results in the present study are in good agreement with the results in Shen and Xiang.[15,18]

Table 4 compares the Young's modulus obtained from the rule of mixtures and MD simulations[55] with material properties of the matrices and CNTs efficiency parameters shown in Tables 2 and 3. It is clear that the Young's modulus results are the same when using CNTs efficiency parameters for the rule of mixtures, as shown in Table 4.

Table 4. Comparison of elastic modulus for PMMA/CNT and PmPV/CNT composites reinforced by (10, 10) SWCNT.

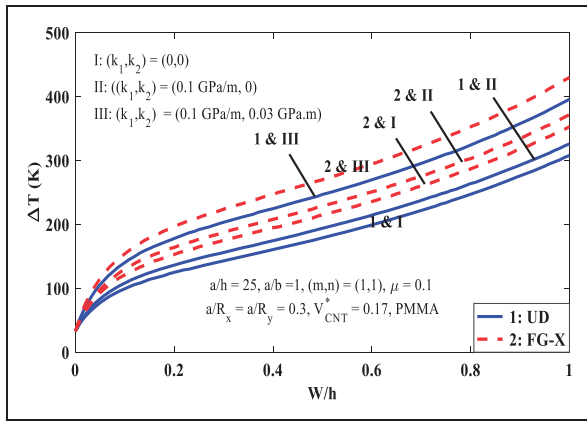|		MD[56]		Rule of mixtures			
	V_{CNT}^*	E_{11} (GPa)	E_{22} (GPa)	E_{11} (GPa)	E_{22} (GPa)	η_1	η_2
PMMA/CNT	0.12	94.6	2.9	95.0	2.9	0.137	1.022
composites	0.17	138.9	4.9	138.4	4.9	0.142	1.626
	0.28	224.2	5.5	224.7	5.5	0.141	1.585
PmPV/CNT	0.11	94.8	2.2	94.4	2.2	0.149	0.934
composites	0.14	120.2	2.3	120.4	2.3	0.150	0.941
	0.17	145.6	3.5	144.8	3.5	0.149	1.381

Figure 5. Effect of foundation model on the thermal post-buckling behavior of nanocomposite double-curved shallow shells with the PMMA matrix.
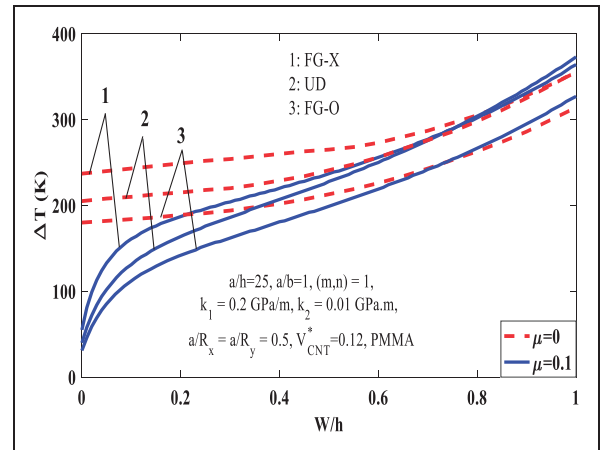

Figure 7. Effect of different types of CNTs on the thermal post-buckling behavior of nanocomposite double-curved shallow shells with the PMMA matrix.
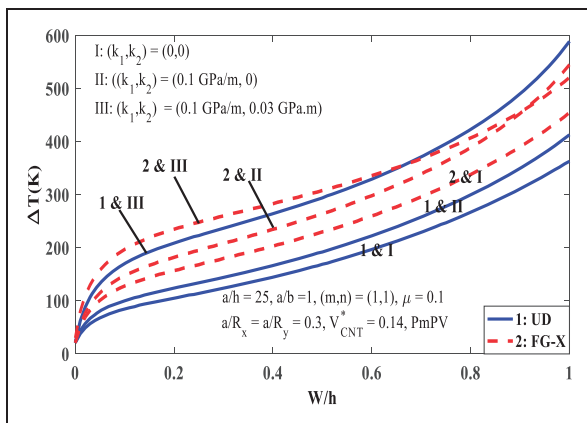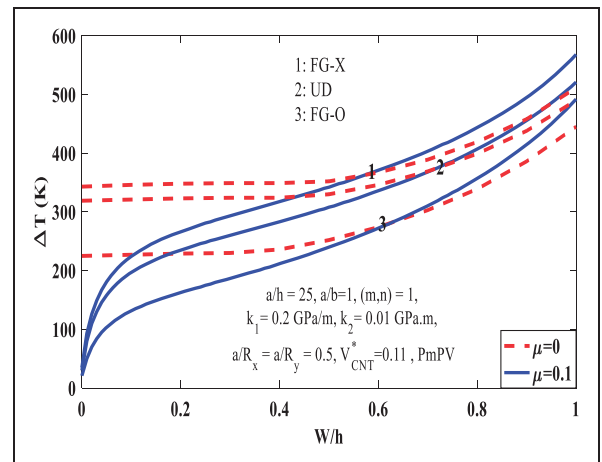

Figure 6. Effect of foundation model on the thermal post-buckling behavior of nanocomposite double-curved shallow shells with the PMMA matrix.

Figure 8. Effect of different types of CNTs on the thermal post-buckling behavior of nanocomposite double-curved shallow shells with the PmPV matrix.

Thermal post-buckling results

In this section, numerical results are presented for the nonlinear thermal post-buckling behavior of FG-CNT-reinforced composite double-curved shallow shells with the PMMA and PmPV matrices the material properties of which are shown in Tables 2 and 3. The geometrical parameters of FG-CNT-reinforced composite double-curved shallow shells are shown in detail in Figures 5 to 12.

Figures 5 and 6 compare the influences of Winker foundation model and Pasternak foundation model on the thermal post-buckling behavior of FG-CNT double-curved shallow shells with two different matrices. In these figures, the double-curved shallow shells are examined with three cases without elastic foundations $(K_w, K_p) = (0, 0)$, the Winkler foundation model $(K_w, K_p) = (0.1, 0)$, and the Pasternak foundation model $(K_w, K_p) = (0.1, 0.03)$. It can be seen that the elastic foundations have significantly affected the thermal post-buckling strength of double-curved shallow shells increases.

The effect of three various types of CNTs on the thermal post-buckling behavior of nanocomposite double-curved shallow shells with PMMA matrix (Figure 7) and PmPV matrix (Figure 8) are observed. The geometrical parameters of the double-curved shallow shells are shown in these figures. It is clear that the thermal post-buckling strength of FG-X CNT-reinfoced composite double-curved shallow shells is the highest when $Wh < 0.6$ (Figure 6) and $Wh < 1$ (Figure 7). The thermal post-buckling strength of UD CNT-reinforced composite double-curved shallow shells is slightly lower than the FG-X type and the thermal post-buckling strength of FG-O type is the lowest among the three types.

Figures 9 and 10 illustrate the effect of CNTs volume fraction on the post-buckling behavior of nanocomposite double-curved shallow shells with PMMA and PmPV matrices, respectively. In Figure 9, three different sets of CNTs volume fraction $V_{CNT}^* = (0.12, 0.17, 0.28)$ are examined. The thermal post-buckling strength
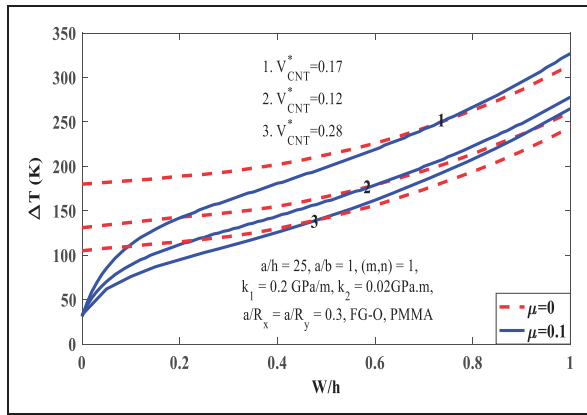
Figure 9. Effect of volume fractions of CNTs on the thermal post-buckling behavior of nanocomposite double-curved shallow shells with PMMA matrix.
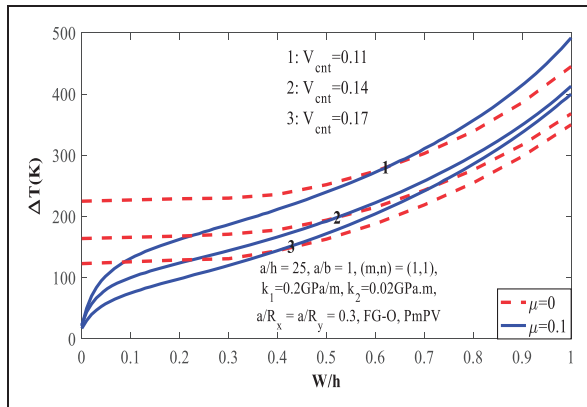

Figure 11. Effect of ratio a/b on the thermal post-buckling behavior of nanocomposite double-curved shallow shells reinforced by CNTs.

Figure 10. Effect of volume fractions of CNTs on the thermal post-buckling behavior of nanocomposite double-curved shallow shells with PmPV matrix.

Figure 12. Effect of length-to-radius ratio a/R_x on the thermal post-buckling behavior of nanocomposite double-curved shallow shells reinforced by CNTs.

of the double-curved shallow shell with $V_{CNT}^* = 0.17$ is the highest. Meanwhile, the thermal post-buckling strength of the double-curved shallow shell with $V_{CNT}^* = 0.28$ is the lowest. In Figure 10, the post-buckling behavior of nanocomposite double-curved shallow shells with PmPV matrices are considered with three cases of CNTs volume fraction $V_{CNT}^* = (0.11, 0.14, 0.17)$. As can be seen, the thermal post-buckling strength of the double-curved shallow shells increases when CNTs volume fraction increases. The thermal post-buckling strength of the double-curved shallow shell with $V_{CNT}^* = 0.17$ is the highest. The thermal post-buckling strength of the double-curved shallow shell with $V_{CNT}^* = 0.14$ is lower and the thermal post-buckling strength of the shell with $V_{CNT}^* = 0.11$ is the lowest.

Figure 11 shows the effect of a/b ratio on the thermal post-buckling behavior of FG-CNT-reinforced composite double-curved shallow shells. Three cases of ratio $a/b = (1, 1.5, 3)$ are considered. A gradual increase on the thermal post-buckling strength of nanocomposite double-curved shallow shells can be seen when a/b ratio increases and vice versa.
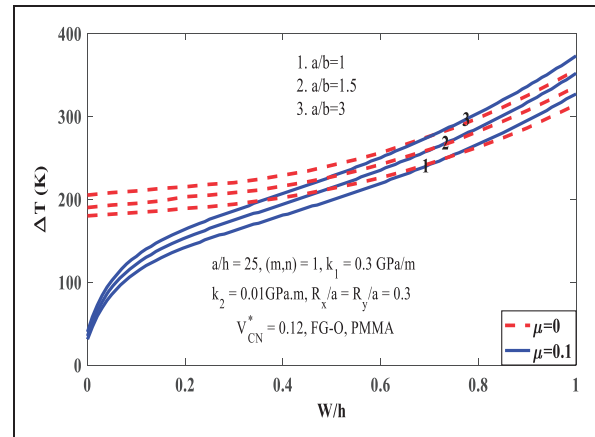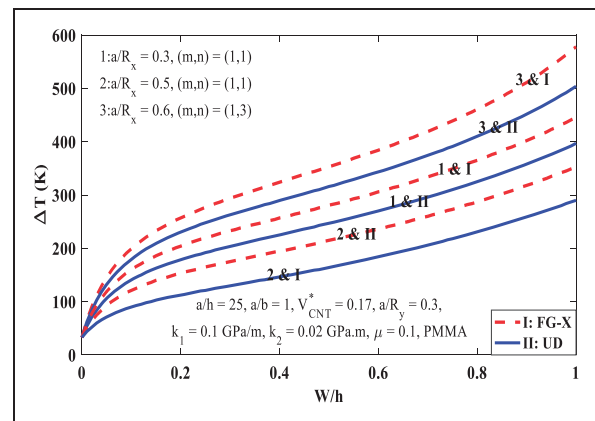
Figure 12 compares the effect of length to radius ($a/R_x = (0.3, 0.5, 0.6)$) on the post-buckling behavior of FG-CNT-reinforced composite double-curved shallow shells. It is found that when a/R_x ratio is increased, the thermal post-buckling load–deflection curve becomes lower and vice versa. The post-buckling curve shows the post-buckling strength of FG-CNT-reinforced composite double-curved shallow shells. In other words, a/R_x increase makes the shells thinner, which results in the lower load capacity of the shells. As can be seen, the thermal post-buckling strength of FG-X CNT-reinforced composite double-curved shallow shell is higher than UD CNT-reinforced composite double-curved shallow shell.

Mechanical post-buckling results

Numerical results are presented in this section for the nonlinear mechanical post-buckling behavior of FG-CNT-reinforced composite double-curved shallow shells. PMMA is chosen as the matrix of the double-curved shallow shells and the material
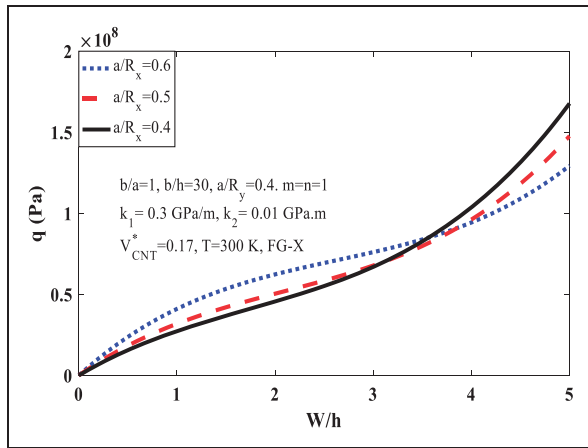
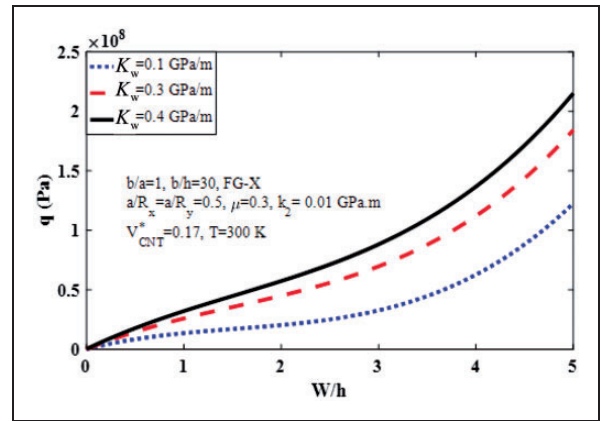**Figure 13.** Effect of a/R_x ratio on the load–deflection curves of nanocomposite double-curved shallow shells.

Figure 15. Effect of the foundation stiffness K_w on the load–deflection curves of nanocomposite double-curved shallow shells.
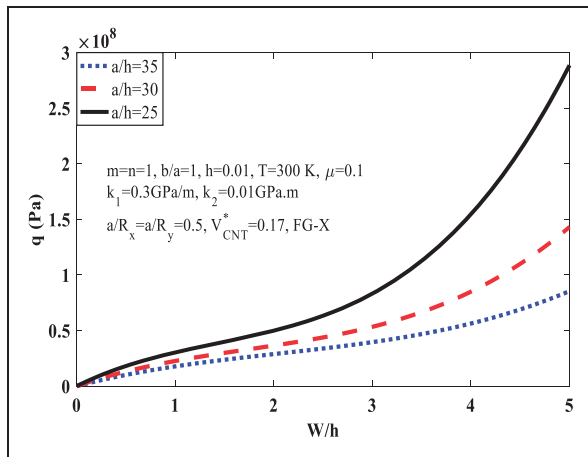

Figure 14. Effect of a/h ratio on the load–deflection curves of nanocomposite double-curved shallow shells.
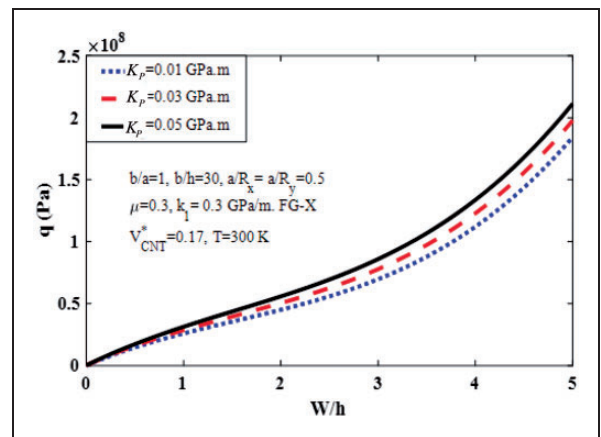

Figure 16. Effect of the foundation stiffness K_P on the load–deflection curves of nanocomposite double-curved shallow shells.

properties are shown in Tables 2 and 3. The geometrical parameters of the double-curved shallow shells are shown detail in Figures 13 to 17.

Figure 13 shows the influences of ratio a/R_x on the mechanical post-buckling load–deflection curves of nanocomposite double-curved shallow shells reinforced by CNTs. Three different sets of ratio $a/R_x = (0.4, 0.5, 0.6)$ are considered. It is clear that there is a fluctuating increase of the mechanical post-buckling strength for three cases. In addition, the mechanical post-buckling strength of the double-curved shallow shell increases when ratio a/R_x increases with $W/h < 3.5$.

Figure 14 shows the effect of length-to-thickness ratio on the mechanical post-buckling behavior of FG-CNT-reinforced composite double-curved shallow shells. Three different values of length-to-thickness ratio ($a/h = (25, 30, 35)$) are considered. It is noticeable that the increase in a/h leads to the mechanical post-buckling load–deflection curve to become lower and vice versa. That is correct because a/h increase makes the FG-CNT-reinforced composite double-curved
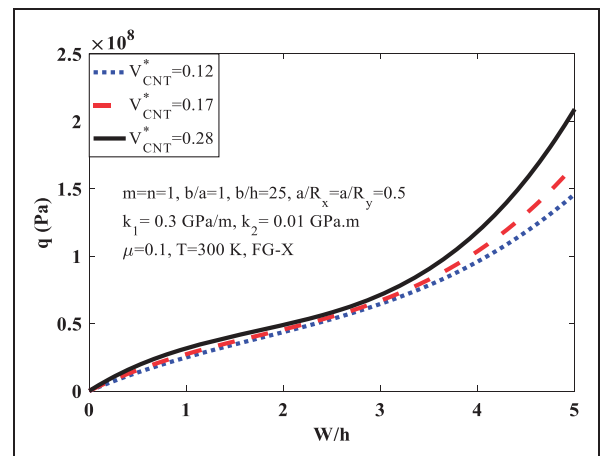

Figure 17. Effect of volume fractions of CNTs on the load–deflection curves of nanocomposite double-curved shallow shells.

shallow shell to become thinner and the mechanical post-buckling strength is decreased.

Figures 15 and 16 show the effect of the foundation stiffness K_w and K_p on the load–deflection curves of nanocomposite double-curved shallow shells. It is noticed that the foundation stiffness have a positive effect in making the capacity load of FG-CNT-reinforced composite double-curved shallow shells to become better. In addition, the capacity load of nanocomposite double-curved shallow shells reinforced by CNTs increases when the foundation stiffness increases.

Figure 17 illustrates the effect of CNTs volume fractions on the load–deflection curves of FG-CNT-reinforced composite double-curved shallow shells. Three cases of CNTs volume fraction are considered $V^*_{CNT} = (0.12, 0.17, 0.28)$. As can be seen, CNTs volume fraction can enhance the post-buckling strength of the double-curved shallow shells.

Concluding remarks

This work aims to analyze the nonlinear mechanical and thermal post-buckling behavior of nanocomposite double-curved shallow shells reinforced by CNTs. Based on the HSDT to derive the formulations with von Karman geometrical nonlinearity, the nonlinear mechanical and thermal post-buckling behavior are obtained by using the Galerkin's method and Airy's stress function. The effect of geometrical and material parameters on the nonlinear mechanical and thermal post-buckling behavior of nanocomposite double-curved shallow shells is examined. The following conclusions can be obtained from this study:

- CNTs do wonders for the stiffness of nanocomposite double-curved shallow shells.
- The mechanical and thermal post-buckling strength of nanocomposite double-curved shallow shells are considerabaly affected by various types of CNT distributions. The mechanical and thermal post-buckling strength of FG-X CNT-reinfoced composite double-curved shallow shells is the highest.
- The elastic foundations significantly affected the mechanical and thermal post-buckling behavior of nanocomposite double-curved shallow shells reinforced by CNTs. In addition, the effect of Pasternak elastic foundation is significantly stronger than the Winkler elastic foundation.
- The geometrical parameters have effects on the nonlinear mechanical and thermal post-buckling behavior of nanocomposite double-curved shallow shells reinforced by CNTs.

Declaration of Conflicting Interests

The author(s) declared no potential conflicts of interest with respect to the research, authorship, and/or publication of this article.

ORCID iD

Nguyen Dinh Duc http://orcid.org/0000-0003-2656-7497

References

1. Yu MF, Lourie O, Dyer MJ, et al. Strength and breaking mechanism of multiwalled carbon nanotubes under tensile load. *Science* 2000; 287: 637–640.
2. Peng B, Locascio M, Zapol P, et al. Measurements of near-ultimate strength for multiwalled carbon nanotubes and irradiation-induced crosslinking improvements. *Nat Nanotechnol* 2008; 3: 626–631.
3. Pantano A and Cappello F. Numerical model for composite material with polymer matrix reinforced by carbon nanotubes. *Meccanica* 2008; 43: 263–270.
4. Collins PG and Avouris P. Nanotubes for electronics. *Sci Am* 2000; 283: 62–29.
5. Charlier JC, Blase X and Roche S. Electronic and transport properties of nanotubes. *Rev Mod Phys* 2007; 79: 677–732.
6. Thostenson ET, Li C and Chou TW. Nanocomposites in context. *Compos Sci Technol* 2005; 65: 491–516.
7. Ding H, Chen S-J and Cheng K. The atomic-scale finite-element modelling of single-walled carbon nanotubes. *Proc IMechE, Part C: J Mechanical Engineering Science* 2007; 221: 613–617.
8. Shen HS. Nonlinear bending of functionally graded carbon nanotube reinforced composite plates in thermal environments. *Compos Struct* 2009; 91: 9–19.
9. Shen HS and Zhang CL. Thermal buckling and post-buckling behavior of functionally graded carbon nanotube-reinforced composite plates. *Mater Des* 2010; 31: 3403–3411.
10. Shen HS and Zhu ZH. Buckling and postbuckling behavior of functionally graded nanotube-reinforced composite plates in thermal environments. *Comput Mater Continua* 2010; 18: 155–182.
11. Wang ZX and Shen HS. Nonlinear vibration of nanotube-reinforced composite plates in thermal environments. *Comput Mater Sci* 2011; 50: 2319–2330.
12. Shen HS and Xiang Y. Postbuckling of nanotube-reinforced composite cylindrical shells under combined axial and radial mechanical loads in thermal environment. *Compos Part B: Eng* 2013; 52: 311–322.
13. Shen HS and Xiang Y. Nonlinear vibration of nanotube-reinforced composite cylindrical shells in thermal environments. *Comput Methods Appl Mech Eng* 2012; 213–216: 196–205.
14. Shen HS and Xiang Y. Postbuckling of axially compressed nanotube-reinforced composite cylindrical panels resting on elastic foundations in thermal environments. *Compos Part B: Eng* 2014; 67: 50–61.
15. Shen HS and Xiang Y. Thermal postbuckling of nanotube-reinforced composite cylindrical panels resting on elastic foundations in thermal environments. *Compos Struct* 2015; 123: 383–392.
16. Shen HS and Xiang Y. Nonlinear response of nanotube-reinforced composite cylindrical panels subjected

to combined loadings and resting on elastic foundations. *Compos Struct* 2015; 131: 939–950.

17. Shen HS. Thermal buckling and postbuckling behavior of functionally graded carbon nanotube-reinforced composite cylindrical shells. *Compos Part B: Eng* 2012; 43: 1030–1038.

18. Shen HS and Xiang Y. Postbuckling of pressure-loaded nanotube-reinforced composite doubly curved panels resting on elastic foundations in thermal environments. *Mech Sci* 2016; 107: 225–234.

19. Enrique GM, Luis RT, Rafael CT, et al. Buckling analysis of functionally graded carbon nanotube-reinforced curved panels under axial compression and shear. *Compos Part B: Eng* 2017; 108: 243–256.

20. Duc ND, Quan TQ and Khoa ND. New approach to investigate nonlinear dynamic response and vibration of imperfect functionally graded carbon nanotube reinforced composite double curved shallow shells subjected to blast load and temperature. *Aerosp Sci Technol* 2017; 71: 360–372.

21. Mirzaei M and Kiani Y. Free vibration of functionally graded carbon nanotube reinforced composite cylindrical panels. *Compos Struct* 2016; 142: 45–56.

22. Kiani Y. Free vibration of FG-CNT reinforced composite spherical shell panels using Gram-Schmidt shape functions. *Compos Struct* 2017; 159: 368–381.

23. Kiani Y. Dynamics of FG-CNT reinforced composite cylindrical panel subjected to moving load. *Thin-Walled Struct* 2017; 111: 48–57.

24. Kiani Y, Dimitri R and Tornabene F. Free vibration of FG-CNT reinforced composite skew cylindrical shells using the Chebyshev-Ritz Formulation. *Compos Part B: Eng* 2018; 147: 169–177.

25. Zhang LW, Lei ZX, Liew KM, et al. Static and dynamic of carbon nanotube reinforced functionally graded cylindrical panels. *Compos Struct* 2014; 111: 205–212.

26. Zhang LW, Lei ZX, Liew KM, et al. Large deflection geometrically nonlinear analysis of carbon nanotube-reinforced functionally graded cylindrical panels. *Comput Methods Appl Mech Eng* 2014; 273: 1–18.

27. Zhang LW, Song ZG, Qiao P, et al. Modeling of dynamic responses of CNT-reinforced composite cylindrical shells under impact loads. *Comput Methods Appl Mech Eng* 2017; 313: 889–903.

28. Zghal S, Frikha A and Dammak F. Free vibration analysis of carbon nanotube-reinforced functionally graded composite shell structures. *Appl Math Model* 2018; 53: 132–155.

29. Pouresmaeeli S, Fazelzadeh SA, Ghavanloo E, et al. Uncertainty propagation in vibrational characteristics of functionally graded carbon nanotube-reinforced composite shell panels. *Int J Mech Sci*. Epub ahead of print 2017. DOI: 10.1016/j.ijmecsci.2017.05.049.

30. Duc ND and Nguyen PD. The dynamic response and vibration of functionally graded carbon nanotubes reinforced composite (FG-CNTRC) truncated conical shells resting on elastic foundation. *Materials* 2017; 10: 1194.

31. Duc ND, Cong PH, Tuan ND, et al. Thermal and mechanical stability of functionally graded carbon nanotubes (FG CNT)-reinforced composite truncated conical shells surrounded by the elastic foundations. *Thin-Walled Struct* 2017; 115: 300–310.

32. Asadi H. Numerical simulation of the fluid-solid interaction for CNT reinforced functionally graded cylindrical shells in thermal environments. *Acta Astronaut* 2017; 138: 214–224.

33. Trang LTN and Tung HV. Thermalmechanical nonlinear analysis of axially compressed carbon nanotube-reinforced composite cylindrical panels resting on elastic foundations with tangentially restrained edges. *J Therm Stress* 2017; 41: 418–438.

34. Ansari R, Pourashraf T, Gholami R, et al. Analytical solution for nonlinear post-buckling of functionally graded carbon nanotube-reinforced composite shells with piezoelectric layers. *Compos Part B: Eng* 2018; 90: 267–277.

35. Alibeigloo A and Pasha AAZ. Thermo-electro-elasticity solution of functionally graded carbon nanotube reinforced composite cylindrical shell embedded in piezoelectric layers. *Compos Struct* 2017; 173: 268–280.

36. Ninh DG and Bich DH. Characteristics of nonlinear vibration of nanocomposite cylindrical shells with piezoelectric actuators under thermo-mechanical loads. *Aerosp Sci Technol* 2018; 77: 595–609.

37. Lin H, Cao D, Shao C, et al. Studies for aeroelastic characteristics and nonlinear response of FG-CNT reinforced composite panel considering the transient heat conduction. *Compos Struct* 2018; 188: 470–482.

38. Cheo K, Wang Q, Tang J, et al. Vibration analysis for coupled composite laminated axis-symmetric doubly-curved revolution shell structures by unified Jacobi-Ritz method. *Compos Struct* 2018; 194: 136–157.

39. Guo JH, Shi DY, Wang QS, et al. Dynamic analysis of laminated doubly-curved shells with general boundary conditions by means of a domain decomposition method. *Int J Mech Sci* 2018; 138–139: 159–186.

40. Duc ND, Kim SE, Cong HP, et al. Dynamic response and vibration of composite double curved shallow shells with negative Poisson's ratio in auxetic honeycombs core layer on elastic foundations subjected to blast and damping loads. *Int J Mech Sci* 2017; 133: 504–512.

41. Duc ND, Cong HP, Khanh ND, et al. New approach to investigate nonlinear dynamic response of sandwich auxetic double curves shallow shells using TSDT. *Compos Struct* 2018; 185: 455–465.

42. Biglari H and Jafari AA. Static and free vibration analyses of doubly curved composite sandwich panels with soft core based on a new three-layered mixed theory. *Proc IMechE, Part C: J Mechanical Engineering Science* 2010; 224: 2332–2349.

43. Monterrubio LE. Free vibration of shallow shells using the Rayleigh–Ritz method and penalty parameters. *Proc IMechE, Part C: J Mechanical Engineering Science* 2009; 223: 2263–2272.

44. Brischetto S and Tornabene F. Advanced GDQ models and 3D stress recovery in multilayered plates, spherical and double-curved panels subjected to transverse shear loads. *Compos Part B: Eng* 2018; 146: 224–269.

45. Talebitooti R and Zarastvand M. The effect of nature of porous material on diffuse field acoustic transmission of the sandwich aerospace composite doubly curved shell. *Aerosp Sci Technol* 2018; 78: 157–170.

46. Mohammad A. Analysis of a doubly curved piezoelectric nano shell: nonlocal electro-elastic bending solution. *Eur J Mech-A/Solids* 2018; 70: 226–237.

47. Sirivolu D and Hoo Falt MS. Dynamic stability of double-curvature composite shells under external blast. *Int J Nonlinear Mech* 2015; 77: 281–290.

48. Chen H, Wang A, Hao Y, et al. Free vibration of FGM sandwich doubly-curved shallow shell based on a new shear deformation theory with stretching effects. *Compos Struct* 2017; 179: 50–60.

49. Duc ND and Quan TQ. Nonlinear thermal stability of eccentrically stiffened FGM double curved shallow shells. *J Therm Stress* 2017; 40: 211–236.

50. Duc ND and Quan TQ. Nonlinear dynamic analysis of imperfect functionally graded material double curved shallow shells with temperature-dependent properties on elastic foundation. *J Vib Control* 2013; 21: 1340–1362.

51. Pang F, Li H, Wang X, et al. A semi analytical method for the free vibration of doubly-curved shells of revolution. *Comput Math Appl* 2018; 75: 3249–3268.

52. Zare JF, Mohammadi DP, Dimitri R, et al. First-order shear deformation theory for orthotropic doubly-curved shells based on a modified couple stress elasticity. *Aerosp Sci Technol* 2018; 73: 129–147.

53. Kateryna D and Nataliia K. Stress-deformable state of isotropic double curved shell with internal cracks and a circular hole. *Mech Mater* 2015; 90: 111–117.

54. Reddy JN. *Mechanics of laminated composite plates and shells*. Boca Raton, FL: CRC Press, 2004.

55. Han Y and Elliott J. Molecular dynamics simulations of the elastic properties of polymer/carbon nanotube composites. *Comput Mater Sci* 2007; 39: 315–323.

Appendix 1

$$U_{11} = A_{44} - 6c_1 D_{44} + 9c_1^2 H_{44},$$
$$U_{12} = A_{55} - 6c_1 D_{55} + 9c_1^2 H_{55},$$
$$U_{13} = -c_1^2 (F_{11} I_{15} + F_{12} I_{25} + O_{11}),$$
$$U_{14} = -c_1^2 (4F_{66} I_{33} + 4O_{66} + F_{11} I_{16} + F_{12} I_{26} + 2O_{12} + F_{12} I_{15} + F_{22} I_{25}),$$
$$U_{15} = -c_1^2 (F_{12} I_{16} + F_{22} I_{26} + O_{22}),$$
$$U_{16} = c_1 (F_{11} I_{13} - c_1 F_{11} I_{15} + H_{11} - c_1 O_{11} + F_{12} I_{23} - c_1 F_{12} I_{25}),$$
$$U_{17} = c_1 (2F_{66} I_{32} - 2c_1 F_{66} I_{33} + 2H_{66} - 2c_1 O_{66} + c_1 F_{12} I_{13} - c_1 F_{12} I_{15} + H_{12} - c_1 O_{12} + F_{22} I_{23} - c_1 F_{22} I_{25}),$$
$$U_{18} = c_1 (F_{12} I_{14} - c_1 F_{12} I_{16} + F_{22} I_{24} - c_1 F_{22} I_{26} + H_{22} - c_1 O_{22}),$$
$$U_{19} = c_1 (2F_{66} I_{32} - 2c_1 F_{66} I_{33} + 2H_{66} - 2c_1 O_{66} + F_{11} I_{14} - c_1 F_{11} I_{16} + F_{12} I_{24} - c_1 F_{12} I_{26} + H_{12} - c_1 O_{12}),$$
$$U_{110} = -c_1 (F_{11} I_{12} - F_{12} I_{21}),$$
$$U_{111} = -c_1 (2F_{66} I_{31} - F_{11} I_{11} + 2F_{12} I_{12} - F_{22} I_{21}),$$
$$U_{112} = c_1 (F_{12} I_{11} - F_{22} I_{12})$$

$$U_{21} = -A_{44} + 6c_1 D_{44} - 9c_1^2 H_{44},$$
$$U_{22} = -c_1 (B_{11} I_{15} + H_{11} + B_{12} I_{25} - c_1 F_{11} I_{15} - c_1 O_{11} - c_1 F_{12} I_{25}),$$
$$U_{23} = -c_1 (B_{11} I_{16} + B_{12} I_{26} + H_{12} + 2B_{66} I_{33} + 2H_{66} - 2c_1 F_{66} I_{33} - 2c_1 O_{66} - c_1 F_{11} I_{16} - c_1 F_{12} I_{26} - c_1 O_{12}),$$
$$U_{24} = B_{11} I_{13} - c_1 B_{11} I_{15} + D_{11} - c_1 H_{11} + B_{12} I_{23} - c_1 B_{12} I_{25} - c_1 F_{11} I_{13} + c_1^2 F_{11} I_{15} - c_1 H_{11} + c_1^2 O_{11} - c_1 F_{12} I_{23} + c_1^2 F_{12} I_{25},$$
$$U_{25} = B_{66} I_{32} - c_1 B_{66} I_{33} + D_{66} - c_1 H_{66} - c_1 F_{66} I_{32} + c_1^2 F_{66} I_{33} - c_1 H_{66} + c_1^2 O_{66},$$
$$U_{26} = \begin{pmatrix} B_{11} I_{14} - c_1 B_{11} I_{16} + B_{12} I_{24} - c_1 B_{12} I_{26} \\ +D_{12} - c_1 H_{12} + B_{66} I_{32} - c_1 B_{66} I_{33} \\ +D_{66} - c_1 H_{66} - c_1 F_{66} I_{32} + c_1^2 F_{66} I_{33} \\ -c_1 H_{66} + c_1^2 O_{66} - c_1 F_{11} I_{14} + c_1^2 F_{11} I_{16} \\ -c_1 F_{12} I_{24} + c_1^2 F_{12} I_{26} - c_1 H_{12} + c_1^2 O_{12} \end{pmatrix},$$
$$U_{27} = -B_{11} I_{12} + B_{12} I_{21} + c_1 F_{11} I_{12} - c_1 F_{12} I_{21},$$
$$U_{28} = B_{11} I_{11} - B_{12} I_{12} - B_{66} I_{31} - c_1 F_{11} I_{11} + c_1 F_{12} I_{12} + c_1 F_{66} I_{31}$$

$$U_{31} = -A_{55} + 6c_1 D_{55} - 9c_1^2 H_{55},$$
$$U_{32} = -c_1 \begin{pmatrix} 2B_{66} I_{33} + 2H_{66} + B_{12} I_{15} + H_{12} \\ +B_{22} I_{25} - 2c_1 F_{66} I_{33} - 2c_1 O_{66} \\ -c_1 F_{12} I_{15} - c_1 O_{12} - c_1 F_{22} I_{25} \end{pmatrix},$$
$$U_{33} = -c_1 (B_{12} I_{16} + B_{22} I_{26} + H_{22} - c_1 F_{12} I_{16} - c_1 F_{22} I_{26} - c_1 O_{22}),$$
$$U_{34} = \begin{pmatrix} B_{66} I_{32} - c_1 B_{66} I_{33} + D_{66} - c_1 H_{66} + B_{12} I_{13} \\ -c_1 B_{12} I_{15} + D_{12} - c_1 H_{12} + B_{22} I_{23} \\ -c_1 B_{22} I_{25} - c_1 F_{66} I_{32} + c_1^2 F_{66} I_{33} \\ -c_1 H_{66} + c_1^2 O_{66} - c_1 F_{12} I_{13} + c_1^2 F_{12} I_{15} \\ -c_1 H_{12} + c_1^2 O_{12} - c_1 F_{22} I_{23} + c_1^2 F_{22} I_{25} \end{pmatrix},$$
$$U_{35} = B_{66} I_{32} - c_1 B_{66} I_{33} + D_{66} - c_1 H_{66} - c_1 F_{66} I_{32} + c_1^2 F_{66} I_{33} - c_1 H_{66} + c_1^2 O_{66},$$
$$U_{36} = \begin{pmatrix} B_{12} I_{14} - c_1 B_{12} I_{16} + B_{22} I_{24} - c_1 B_{22} I_{26} \\ +D_{22} - c_1 H_{22} - c_1 F_{12} I_{14} + c_1^2 F_{12} I_{16} \\ -c_1 F_{22} I_{24} + c_1^2 F_{22} I_{26} - c_1 H_{22} + c_1^2 O_{22}, \end{pmatrix},$$
$$U_{37} = -B_{66} I_{31} - B_{12} I_{12} + B_{22} I_{21} + c_1 F_{66} I_{31} + c_1 F_{12} I_{12} - c_1 F_{22} I_{21},$$
$$U_{38} = B_{12} I_{11} - B_{22} I_{12} - c_1 F_{12} I_{11} + c_1 F_{22} I_{12}$$

Appendix 2

$$l_{11} = -k_1 - k_2 (\lambda_m^2 + \delta_n^2) + U_{13} \lambda_m^4 + U_{14} \lambda_m^2 \delta_n^2 + U_{15} \delta_n^4 + U_{110} P_1 \lambda_m^4 + U_{111} P_1 \lambda_m^2 \delta_n^2 + U_{112} P_1 \delta_n^4 - P_1 \left(\frac{\lambda_m^2}{R_y} + \frac{\delta_n^2}{R_x} \right),$$
$$l_{12} = -U_{11} \lambda_m + U_{16} \lambda_m^3 + U_{17} \lambda_m \delta_n^2 + U_{110} P_2 \lambda_m^4 + U_{111} P_2 \lambda_m^2 \delta_n^2 + U_{112} P_2 \delta_n^4$$

$$- P_2\left(\frac{\lambda_m^2}{R_y} + \frac{\delta_n^2}{R_x}\right),$$

$$l_{13} = -U_{12}\delta_n + U_{18}\delta_n^3 + U_{19}\lambda_m^2\delta_n$$
$$+ U_{110}P_3\lambda_m^4 + U_{111}P_3\lambda_m^2\delta_n^2 + U_{112}P_3\delta_n^4$$
$$- P_3\left(\frac{\lambda_m^2}{R_y} + \frac{\delta_n^2}{R_x}\right),$$

$$l_{14} = \frac{32P_2\lambda_m\delta_n}{3ab}, \quad l_{15} = \frac{32P_3\lambda_m\delta_n}{3ab},$$

$$l_{21} = -\lambda_m^3(U_{22} + P_1U_{27}) - \lambda_m\delta_n^2(U_{23} + P_1U_{28}),$$

$$l_{22} = U_{21} - U_{24}\lambda_m^2 - U_{25}\delta_n^2 - U_{27}P_2\lambda_m^3$$
$$- U_{28}P_2\lambda_m\delta_n^2,$$

$$l_{23} = -U_{26}\lambda_m\delta_n - U_{27}P_3\lambda_m^3 - U_{28}P_3\lambda_m\delta_n^2,$$

$$l_{31} = -\lambda_m^2\delta_n(U_{32} + P_1U_{37}) - \delta_n^3(U_{33} + P_1U_{38}),$$

$$l_{32} = -U_{34}\lambda_m\delta_n - U_{38}P_2\delta_n^3 - U_{37}P_2\lambda_m^2\delta_n,$$

$$l_{33} = U_{31} - U_{35}\lambda_m^2 - U_{36}\delta_n^2 - U_{38}P_3\delta_n^3 - U_{37}P_3\lambda_m^2\delta_n$$

$$n_1 = -U_{11}\lambda_m^2 - U_{12}\delta_n^2, \quad n_2 = \frac{32P_1\lambda_m\delta_n}{3ab},$$

$$n_3 = \frac{2\delta_n}{3abI_{21}\lambda_m R_y} + \frac{2\lambda_m}{3abI_{11}\delta_n R_x} - \frac{8U_{110}\lambda_m\delta_n}{3abI_{21}}$$
$$- \frac{8U_{112}\lambda_m\delta_n}{3abI_{11}},$$

$$n_4 = -\frac{\lambda_m^4}{16I_{11}} - \frac{\delta_n^4}{16I_{21}}, \quad n_5 = \frac{16}{mn\pi^2}, \quad n_6 = U_{21}\lambda_m,$$

$$n_7 = \frac{8U_{27}\delta_n}{3abI_{21}}, \quad n_8 = U_{31}\delta_n, \quad n_9 = \frac{8U_{38}\lambda_m}{3abI_{11}}$$

Appendix 3

$$m_1 = \frac{4}{ab}\left(\frac{P_1\delta_n}{\lambda_m} + \frac{c_1\lambda_m K_1}{\delta_n} + \frac{c_1\delta_n K_2}{\lambda_m} + \frac{K_3}{\lambda_m\delta_n}\right),$$

$$m_2 = \frac{4}{ab}\left(\frac{P_2\delta_n}{\lambda_m} - \frac{K_4}{\delta_n} + \frac{c_1 K_1}{\delta_n}\right),$$

$$m_3 = \frac{4}{ab}\left(\frac{P_3\delta_n}{\lambda_m} - \frac{K_5}{\lambda_m} + \frac{c_1 K_2}{\lambda_m}\right), \quad m_4 = -\frac{K_6}{8};$$

$$m_5 = -1; m_6 = 0,$$

$$m_1^* = \frac{4}{ab}\left(\frac{P_1\lambda_m}{\delta_n} + \frac{c_1\lambda_m K_7}{\delta_n} + \frac{c_1\delta_n K_8}{\lambda_m} + \frac{K_9}{\lambda_m\delta_n}\right),$$

$$m_2^* = \frac{4}{ab}\left(\frac{P_2\lambda_m}{\delta_n} - \frac{K_{10}}{\delta_n} + \frac{c_1 K_7}{\delta_n}\right),$$

$$m_3^* = \frac{4}{ab}\left(\frac{P_3\lambda_m}{\delta_n} - \frac{K_{11}}{\lambda_m} + \frac{c_1 K_8}{\lambda_m}\right), \quad m_4^* = -\frac{K_{12}}{8};$$

$$m_5^* = 0; \quad m_6^* = -1$$

$$K_1 = \frac{(I_{12}I_{25} + I_{15}I_{21})}{(I_{12}^2 - I_{11}I_{21})}, \quad K_2 = \frac{(I_{16}I_{21} + I_{12}I_{26})}{(I_{12}^2 - I_{11}I_{21})},$$

$$K_3 = \left(\frac{I_{12}}{R_y} + \frac{I_{21}}{R_x}\right)\frac{1}{(I_{12}^2 - I_{11}I_{21})}, \quad K_4 = \frac{(I_{12}I_{23} + I_{13}I_{21})}{(I_{12}^2 - I_{11}I_{21})}$$

$$K_5 = \frac{(I_{12}I_{24} + I_{14}I_{21})}{(I_{12}^2 - I_{11}I_{21})}, \quad K_6 = \frac{(I_{21}\lambda_m^2 + I_{12}\delta_n^2)}{(I_{12}^2 - I_{11}I_{21})},$$

$$K_7 = \frac{(I_{11}I_{25} + I_{12}I_{15})}{(I_{12}^2 - I_{11}I_{21})}, \quad K_8 = \frac{(I_{11}I_{26} + I_{12}I_{16})}{(I_{12}^2 - I_{11}I_{21})}$$

$$K_9 = \left(\frac{I_{11}}{R_y} + \frac{I_{12}}{R_x}\right)\frac{1}{(I_{12}^2 - I_{11}I_{21})},$$

$$K_{10} = \frac{(I_{11}I_{23} + I_{12}I_{13})}{(I_{12}^2 - I_{11}I_{21})}, \quad K_{11} = \frac{(I_{11}I_{24} + I_{12}I_{14})}{(I_{12}^2 - I_{11}I_{21})},$$

$$K_{12} = \frac{(I_{11}\delta_n^2 + I_{12}\lambda_m^2)}{(I_{12}^2 - I_{11}I_{21})}$$

Appendix 4

$$b_1^1 = -\frac{h^3 B_1}{n_5}, \quad b_1^2 = -\frac{h^2 B_2}{n_5}; \quad b_1^3 = -\frac{h^2 B_3}{n_5},$$

$$b_1^4 = -\frac{h^2 B_4}{n_5}, \quad b_1^5 = -\frac{h B_7}{n_5}, \quad b_1^6 = -\frac{h B_6}{n_5},$$

$$b_1^7 = -\frac{m_5}{R_x}, \quad b_1^8 = -\frac{m_6^*}{R_y}$$

$$b_2^1 = \frac{h B_1}{b_D}, \quad b_2^2 = \frac{B_2}{b_D}, \quad b_2^3 = \frac{B_3}{b_D}, \quad b_2^4 = \frac{B_4}{b_D},$$

$$b_2^5 = \frac{B_5}{b_D h}, \quad b_2^6 = \frac{B_6}{b_D h}, \quad b_2^7 = \frac{n_5 q}{b_D h^2},$$

$$b_D = C_1(W_n + \mu) - \frac{C_2}{h}$$

$$B_1 = \left[\left(l_{14} - m_2\lambda_m^2 - m_2^*\delta_n^2\right)\frac{(n_9 l_{23} - n_7 l_{33})}{(l_{22}l_{33} - l_{23}l_{32})}\right.$$
$$+ \left(l_{15} - m_3\lambda_m^2 - m_3^*\delta_n^2\right)\frac{(n_9 l_{22} - n_7 l_{32})}{(l_{23}l_{32} - l_{22}l_{33})}$$
$$\left. + n_4 - m_4\lambda_m^2 - m_4^*\delta_n^2\right],$$

$$B_2 = \left[\left(l_{14} - m_2\lambda_m^2 - m_2^*\delta_n^2\right)\frac{(n_8 l_{23} - n_6 l_{33})}{(l_{22}l_{33} - l_{23}l_{32})}\right.$$
$$\left. + \left(l_{15} - m_3\lambda_m^2 - m_3^*\delta_n^2\right)\frac{(n_8 l_{22} - n_6 l_{32})}{(l_{23}l_{32} - l_{22}l_{33})}\right]$$

$$B_3 = \left[\left(l_{12} + \frac{n_5 m_2}{R_x} + \frac{n_5 m_2^*}{R_y}\right)\frac{(n_9 l_{23} - n_7 l_{33})}{(l_{22}l_{33} - l_{23}l_{32})}\right.$$
$$+ \left(l_{13} + \frac{n_5 m_3}{R_x} + \frac{n_5 m_3^*}{R_y}\right)\frac{(n_9 l_{22} - n_7 l_{32})}{(l_{23}l_{32} - l_{22}l_{33})}$$
$$\left. + \left(n_3 + \frac{n_5 m_4}{R_x} + \frac{n_5 m_4^*}{R_y}\right)\right],$$

$$B_4 = \left[\left(l_{14} - m_2\lambda_m^2 - m_2^*\delta_n^2\right)\frac{(l_{23}l_{31} - l_{21}l_{33})}{(l_{22}l_{33} - l_{23}l_{32})}\right.$$
$$+ \left(l_{15} - m_3\lambda_m^2 - m_3^*\delta_n^2\right)\frac{(l_{22}l_{31} - l_{21}l_{32})}{(l_{23}l_{32} - l_{22}l_{33})}$$
$$\left. + \left(n_2 - m_1\lambda_m^2 - m_1^*\delta_n^2\right)\right]$$

$$B_5 = \left[\left(l_{12} + \frac{n_5 m_2}{R_x} + \frac{n_5 m_2^*}{R_y} \right) \frac{(n_8 l_{23} - n_6 l_{33})}{(l_{22} l_{33} - l_{23} l_{32})} \right.$$
$$+ \left. \left(l_{13} + \frac{n_5 m_3}{R_x} + \frac{n_5 m_3^*}{R_y} \right) \frac{(n_8 l_{22} - n_6 l_{32})}{(l_{23} l_{32} - l_{22} l_{33})} + n_1 \right],$$

$$B_6 = \left[\left(l_{12} + \frac{n_5 m_2}{R_x} + \frac{n_5 m_2^*}{R_y} \right) \frac{(l_{23} l_{31} - l_{21} l_{33})}{(l_{22} l_{33} - l_{23} l_{32})} \right.$$
$$+ \left(l_{13} + \frac{n_5 m_3}{R_x} + \frac{n_5 m_3^*}{R_y} \right) \frac{(l_{22} l_{31} - l_{21} l_{32})}{(l_{23} l_{32} - l_{22} l_{33})}$$
$$+ \left. \left(l_{11} + \frac{n_5 m_1}{R_x} + \frac{n_5 m_1^*}{R_y} \right) \right]$$

$$B_7 = \left[\left(l_{12} + \frac{n_5 m_2}{R_x} + \frac{n_5 m_2^*}{R_y} \right) \frac{(n_8 l_{23} - n_6 l_{33})}{(l_{22} l_{33} - l_{23} l_{32})} \right.$$
$$+ \left(l_{13} + \frac{n_5 m_3}{R_x} + \frac{n_5 m_3^*}{R_y} \right) \frac{(n_8 l_{22} - n_6 l_{32})}{(l_{23} l_{32} - l_{22} l_{33})}$$
$$+ \left. \left(n_1 - m_5 \lambda_m^2 N_x^T - m_6^* \delta_n^2 N_y^T \right) \right]$$

$$C_1 = \left[m_5 (Q_{11} \alpha_{11} + Q_{12} \alpha_{22}) \lambda_m^2 + m_6^* (Q_{12} \alpha_{11} + Q_{22} \alpha_{22}) \delta_n^2 \right],$$
$$C_2 = \left[m_5 (Q_{11} \alpha_{11} + Q_{12} \alpha_{22}) \frac{n_5}{R_x} + m_6^* (Q_{12} \alpha_{11} + Q_{22} \alpha_{22}) \frac{n_5}{R_y} \right]$$